Scanning Microscopy

Volume 10 | Number 1 Article 7

12-23-1995

Characterizing the Outlines of Degraded Fine-Particles by Fractal Dimension

Andrew Hunt
The State University of New York, hunta@vax.cs.hscsyr.edu

David L. Johnson
The State University of New York

Scanning Microscopy Vol. 10, No. 1, 1996 (pages 69-83) 0891-7035/96$5.00+.25
Scanning Microscopy International, Chicago (AMF O'Hare), IL 60666 USA

CHARACTERIZING THE OUTLINES OF DEGRADED FINE-PARTICLES BY FRACTAL DIMENSION

Andrew Hunt* and David L. Johnson[1]

Department of Pathology, SUNY Health Science Center, Syracuse, NY 13210
[1]Department of Chemistry, SUNY College of Environmental Science and Forestry, Syracuse, NY 13210

(Received for publication September 6, 1995 and in revised form December 23, 1995)

Abstract

Fractal dimension has been used extensively as a descriptor of the rugged outlines of fine-particles. Potentially, it may be a useful parameter for characterizing the outlines of fine-particles which have been subjected to some form of chemical degradation. Here, fractal dimension values have been computed for the outlines of microscopic lead fine-particles both before and after weak hydrochloric acid dissolution experiments. Values obtained for the post-dissolution rugged profiles were greater than those of the pristine fracture grains which had a Euclidean form. The profiles of the degraded fine-particles could be characterized by a single fractal dimension value, or they exhibited multifractal behavior. Data from profiles of fine-particle lead from the natural environment of the soil suggest that fractal dimension calculations may provide a useful descriptor for particles which have undergone chemical dissolution and transformation in such an environment.

Key Words: Fractal, fine-particles, lead, scanning electron microscopy, etching, dissolution, bioavailability.

*Address for correspondence:
Andrew Hunt
Department of Pathology,
SUNY Health Science Center,
750 East Adams Street,
Syracuse, NY 13210
Telephone number: (315) 464-7146
FAX number: (315) 464-7130
E.mail: hunta@vax.cs.hscsyr.edu

Introduction

The rugged outlines (boundaries) of many phenomena in the natural environment exhibit a self-similarity irrespective of the scale at which they are observed. A now commonly used descriptor of the roughness of such outlines is the fractal dimension. In essence, fractal dimension describes the space filling ability of these outlines (Mandelbrot, 1982). Studies have shown that variations in the ruggedness of fine-particle profiles result in different fractal dimensions, and this has led to the extensive use of fractal dimension as an outline descriptor in fine-particle research (Kaye, 1989). As a result of its potential usefulness in this capacity, fractal dimension has also been used to define the roughness of fine-particles in a variety of environmental contexts (e.g., Orford and Whalley, 1983; Katrinak *et al.*, 1993).

The fractal dimension of a rugged particle outline can be calculated by measuring the length of the profile at different scales of observation. For self similar profiles, the amount of increase in observed outline length is the same at any scale. A value for the fractal dimension is easily derived from a plot of the outline length against the unit length at which it was measured at various scales. Referred to as a Richardson plot, the slope of the line fitted to the data points on the plot yields the fractal dimension of the boundary (Mandelbrot, 1967).

The value of a grain shape descriptor in the study of fine particles derives from the ability of such a parameter to provide information on particle source based on the rugged nature of its profile. For example, Xie *et al.* (1994) and Kindratenko *et al.* (1994) attempted to characterize airborne particles of different form and origin on the basis of fractal dimension values derived from the particle outlines. Fractal dimension may also, under certain circumstances, provide information on the environmental history of fine-particles. Orford and Whalley (1987) describe the irregular outlines of crushed quartz and carbonate beach sand grains which, under near shore marine conditions, as Kaye (1989) indicates, are likely to undergo mechanical abrasion resulting in a change in shape.

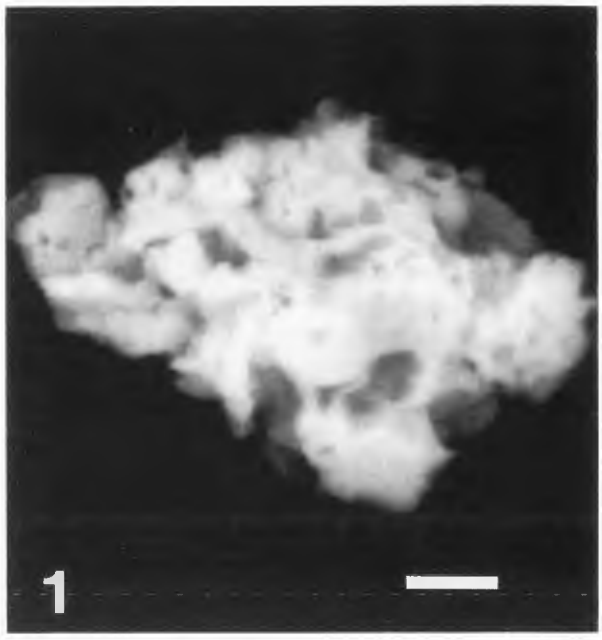

Figure 1. Backscattered electron image of a pitted lead particle from the surface layer of a soil from urban Syracuse, NY. Bar = 1 μm.

In this study, we investigate the rugged profiles of chemically etched lead fine-particles which have been imaged in the scanning electron microscope (SEM). We have previously identified pitted fine particulate lead present in soils sampled from urban sites (Johnson and Hunt, 1995). Lead particles with irregular outlines which are morphologically similar to the grain illustrated in Figure 1 (from the surface layer of a soil in Syracuse, New York), appear to be not uncommon in urban soils (Hunt, unpublished data). The etched and pitted appearance of such grains would suggest that they have been subjected to dissolution conditions in the chemically active environment of the soil. Here, we present some initial findings which assess the degree to which fresh fractured and etched particles can be distinguished on the basis of fractal dimension values obtained from their profiles. In the present study, two types of lead mineral particles have been subjected to acid conditions which are comparable to those in the human stomach. In the absence of airborne automotive lead, uptake for young children, who are particularly sensitive to lead exposure even at low levels, is primarily the result of inadvertent ingestion of soil and dust lead through hand-to-mouth activity. Recently, attention has focused on the bioavailability, following ingestion, of particulate lead present in mine waste contaminated soils which have elevated lead levels (Davis *et al.*, 1992; Ruby *et al.*, 1992; Gulson *et al.*, 1994). Of particular interest has been the possibility that sparingly soluble forms of lead may not be dissolved under weak stomach acid conditions and will enter the intestine in a solid particulate form which cannot be absorbed. Consequently, ingestion of these lead phases would not result in elevated blood lead levels (Cotter-Howells and Thornton, 1991; Davis *et al.*, 1993). Therefore, the behavior of particulate lead under stomach acid conditions is of potential interest.

Material and Methods

Grain profile measurements were made on a number of finely divided lead mineral particles. Two types of lead minerals were used for this purpose, the lead carbonate mineral cerussite ($PbCO_3$), and the lead phosphate mineral pyromorphite ($Pb_5(PO_4)_3Cl$). Cerussite is an orthorhombic-bipyramidal mineral that commonly occurs as prismatic crystals which are soluble in hydrochloric acid and which has a K^*_S value of -2.50 (Rickard and Nriagu, 1978). The chloro-phosphate of lead is a hexagonal-bipyramidal mineral which also dissolves in acid but is less soluble (K^*_S = -25.8). In the first instance, single individual crystals of each mineral were selected and reduced in size by gentle grinding with a mortar and pestle. Fine particle lead that passed through a nylon mesh with a 100 μm opening was used for the analysis. Particulate lead in this size range is comparable with much of the particulate material that adheres to the hands of young children (Duggan and Inskip, 1985).

Surface etching was performed on particles of each mineral type using a dilute solution of hydrochloric acid. In each case, 0.1 N hydrochloric acid was used due to its comparability with the level of acidity in the human stomach (e.g., Day *et al.*, 1979; Rabinowitz, 1993) and thus, permits observations to be made on how fine particulate mineral lead might behave in the stomach of the young child following inadvertent ingestion.

Particle dissolution experiments were conducted in two ways. The *ex situ* experimental method involved suspending the particulate lead in a test tube containing the dilute hydrochloric acid and this suspension was maintained by continuous agitation for some fixed time period. After specific preset time intervals, small volumes of the suspension were removed for analysis. The particulate material extracted from the suspension was immediately added to a larger volume of distilled water which was then drawn across a 0.4 μm pore size polycarbonate membrane filter. To remove all traces of the hydrochloric acid from the particle surfaces, the reservoir of distilled water was refilled twice during the filtration process. Each filter was then attached to a glass microscope slide (specimen mount) with a layer of adhesive carbon paint, and the sample was then evaporatively coated with a thin layer of carbon.

The second form of dissolution experiment was performed *in situ* and initially involved filtering the particulate lead onto a polycarbonate membrane from a distilled water suspension. Again, the filter was mounted on a glass slide support and the particles evaporatively coated with a thin carbon film. In the first instance, individual lead particles of interest were imaged in the SEM and locations of these "target" particles noted. The specimen was then removed from the SEM and the particulate material was treated *in situ* on the filter with the weak acid. This bathing in dilute hydrochloric acid was conducted in two ways. Either, the particulate lead was subjected to a single long period of immersion in the acid or was repeatedly exposed for short periods of time. In the case of the former, the sample was returned to the SEM after the single treatment in order to image the target particles. In the multiple immersion experiments, the specimen was returned to the SEM several times in order to monitor the target grains after each sequential short duration treatment. Immersing the particulate material *in situ* involved pipetting approximately between 0.1 and 0.5 ml of liquid directly onto the filtered material. Following the removal of the reagent, a larger volume of distilled water was immediately pipetted onto the sample (and subsequently removed) to dilute any trace amount of acid remaining on the specimen. Typically, the *in situ* immersion ranged in duration from 15 minutes (for multiple exposure experiments) to 2 hours (for a single treatment) which is roughly equal to the period of time ingested material resides in the stomach before transfer to the upper intestine.

Electron microscopy analysis was performed on an Hitachi (Hitachi Ltd., Tokyo, Japan) S520 SEM interfaced with a PGT (Princeton Gamma-Tech, Princeton, NJ) energy dispersive microanalysis system operating on a Sun Sparc 10 platform (Sun Microsystems, Pleasanton, CA). Imaging was performed in both the secondary electron (SE) and backscattered electron (BE) modes. However, only grain outlines obtained from the BE image were used in subsequent calculations. It was found that in the case of the *in situ* analyses, as the particle progressively dissolved and reduced in size, its outline, as observed in the SE image, became obscured by the intervening carbon coat. Evaporatively coating the specimen with a thin layer of carbon generally appeared not to interfere with the etching process and the coating apparently anchored the particles in place during dissolution. The few grains which were not obviously etched by the acid were generally smaller (approximately 5 μm or less), and/or were platy in form and were deposited flat on the substrate. Rupturing of the carbon coating (allowing the particle to move on the substrate) was only apparent in the case of one large particle ($>$ 50 μm in length) which was not followed continuously throughout the test, but which was subjected to repeated *in situ* immersions in the acid. The BE images of the individual grains were either photographically recorded or stored in digital format after direct capture from the SEM by the linked microanalysis computer. Images in the form of photomicrographs were converted to digital format using a flatbed scanner, and both image types were converted from multiple grey scale to black and white binary images.

Fractal dimensions for grain outlines were computed from the stored binary arrays in a two-stage process. In the first, the image was read into memory, and the maximum circumscribed rectangular dimension was determined for the image. Our Fortran algorithm processed the array in a line scan fashion pixel by pixel, until the first perimeter point was encountered. It then navigated around the boundary between the image and the background creating a sequential list of pixel addresses defining the perimeter of the image until the initial perimeter point was again encountered. Where small scale features on the image were only 1 pixel in width, logic allowed such perimeter points to be counted twice in the process of creating a complete, continuous grain outline. Adjacent perimeter point pixels had coordinate addresses differing by one for x or y, but not for both. This constraint to move around the image perimeter in one of four directions differed from that of Xie *et al.* (1994), by providing a longer distance measure for portions of the perimeter oriented along major diagonals of the feature. The 23 individual particle profiles investigated in this study ranged in length from 1064 to 5566 perimeter points. In stage two, data for the Richardson plots (log perimeter versus log step size) were generated from the sequential perimeter point lists for the outlines by the method of Schwartz and Exner (1980). The perimeter was estimated as the sum of the Euclidean distances between the listed perimeter points. Step size, in this FAST implementation (Hayward *et al.*, 1989) of the Schwartz and Exner (1980) approach, refers to the number of perimeter points in the list between which the distances were computed. The abscissa value used for the Richardson plots as "stride" length was the average step length: total perimeter distance measured, including any remainder less than the specified step size, divided by the number of steps required. All distances were normalized to the maximum length of the circumscribed rectangle for each original image.

Various forms of fine-particle profiles have been observed to produce plots with an identifiable break in the data yielding two straight line segments. The line segment obtained for larger step sizes has a slope which yields a fractal dimension which is referred to by Kaye (1989) and others as the **structural fractal** (δ_S). The value δ_S is considered to be indicative of the large scale

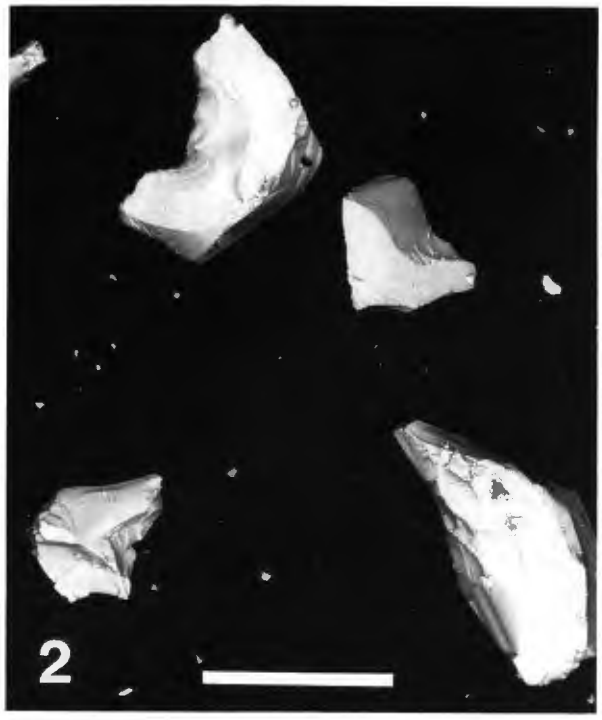

Figure 2. Backscattered electron image of fractured fine-particle cerussite ($PbCO_3$). Bar = 100 μm.

structure of the fine-particle. The characteristics of the fine scale structure of the profile are thought to be defined by the fractal dimension obtained from the slope of the line segment associated with the smaller step sizes. This is referred to as the **textural fractal** (δ_T). In this study, we derived some Richardson plots in which there were no obvious breaks in the data and other plots where there appeared to be very obvious breaks into two (or more) line segments. Consequently, we report values for the fractal dimension for lines fitted to whole data sets (δ) and values for δ_S and δ_T where a break in the data was apparent. The emergence of structural and textural fractals is usually referred to as mixed fractal or multifractal behavior. Following the practical approach advocated elsewhere (Schwartz and Exner, 1980; Orford and Whalley, 1983), the break point in the data set was selected by visual inspection. To obtain values for the slope of the line segments, straight lines were fitted to the Richardson plot data by least squares regression. Plots for the triadic Koch island silhouette, for which δ should be log 4/log 3 $\sim$ 1.262 (Mandlebrot, 1982), using our algorithm gave a fractal dimension of 1.259, and for the Medalia carbon black reference outline (Medalia, 1970-71), bi-fractal dimensions of: 1.12 for the step size 0.035 to 0.132, and 1.33 for the step range 0.132 to 0.530; in good agreement with the values reported by Kaye *et al.* (1987).

Table 1. Fractal dimension values for four pristine cerussite fine-particles.

Main Line Segment δ (r^2)	Lower Line Segment δ (r^2)
1.016 (0.99)	1.070 (0.93)
1.020 (0.98)	1.052 (0.80)
1.015 (0.96)	1.067 (0.64)
1.026 (0.97)	1.071 (0.75)

Results

Ex situ etching of fractured cerussite grains

Cerussite fine-particles were sampled from a dilute hydrochloric acid suspension immediately after immersion (effectively 0 minutes) and after a residence time of 5 minutes, for the purpose of performing profile comparisons. The grains removed at 0 minutes exhibited a typical fractured appearance as illustrated by the four main features in Figure 2. In contrast, after a residence time of 5 minutes in the weak acid, the cerussite fine-particles displayed distinctive rugose outlines (Fig. 3). The highly irregular profile of these etched grains suggests that the dissolution process occurred rapidly across most of the particle surface. While some degree of crystallographic control of the etching process is evident, the degree of roughness indicates active dissolution over much of the grain surface.

The slopes fitted to the Richardson plot data for the etched grains were found to be consistently different from those of the pristine particles. The plots for the large un-etched grains in Figure 2 are characterized by a long flat line segment followed by a shorter, slightly steeper segment at the larger step sizes (Fig. 4). This result is typical for basic Euclidean forms which generate δ values close to unity for the main line segment in the plot (Table 1). The smaller second segment, which is of variable fit (Table 1), emerges when large scale protrusions in the outline lead to a foreshortening in the measured perimeter at larger step sizes. It has been argued by Kaye (1993) that minor large scale projecting features can distort the Richardson plot by producing a "fractal rabbit" (a false fractal emerging from nowhere). Such an artifact can give a misleading indication of outline structure, and Kaye *et al.* (1993) discuss methods for identifying and eliminating fractal rabbits from experimental data. This effect is produced by extended ellipsoidal grain outlines that resemble the cerussite profile set out in Figure 4. In this case, when the step size becomes sufficiently large, part (or all) of the tapering end of the outline will be traversed resulting in an underestimation of the perimeter. In the case of the other

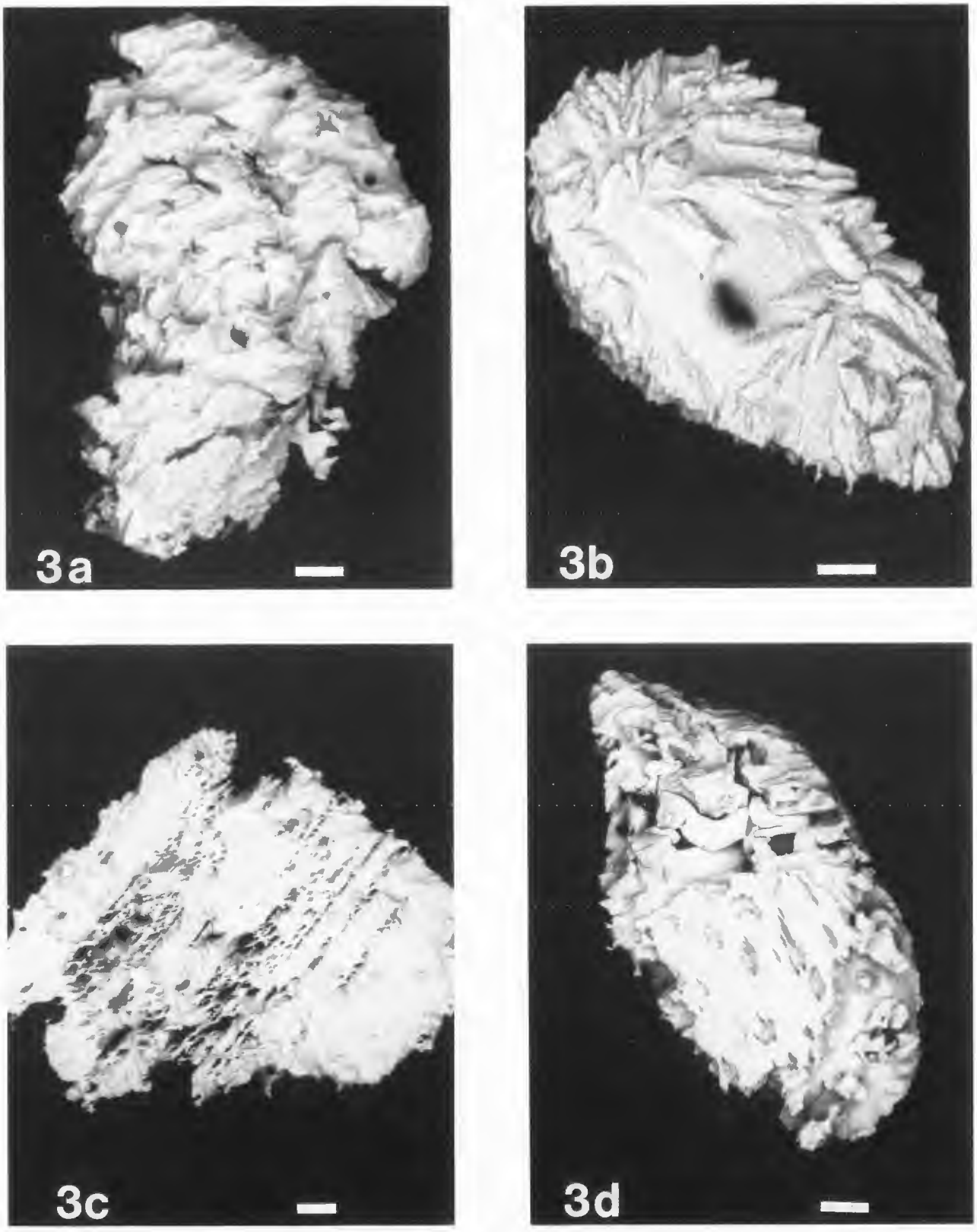

Figure 3. Backscattered electron images of four different cerussite fine-particles sampled from suspension after a residence time of 5 minutes in a solution of 0.1 N HCl. Bars = 10 μm.

Table 2. Fractal dimension values for six cerussite fine-particles etched in a suspension of 0.1 N HCl for 5 minutes.

Single Fractal	Multi-Fractal			
	Texture		Structure	Macro-Form
δ	δ_T (r^2)		δ_S (r^2)	δ_F (r^2)
	δ_{T1} (r^2)	δ_{T2} (r^2)		
1.060 (0.99)	-		-	-
1.108 (0.98)	-		-	-
1.116 (0.98)	-		-	-
-	1.078 (0.99)		1.162 (0.98)	-
-	1.083 (0.99)		-	1.049 (0.92)
-	1.067 (0.98)	1.103 (0.99)	-	1.033 (0.75)

Table 3. Fractal dimension values for two pyromorphite fine-particles before and after immersion in 0.1 N HCl for 2 hours.

Particle	Time (minutes)	δ (r^2)	δ_T (r^2)	δ_S (r^2)
1	0	1.025 (0.89)	-	-
1	120	-	1.050 (0.97)	1.083 (0.95)
2	0	1.021 (0.96)	-	-
2	120	-	1.055 (0.97)	1.144 (0.94)

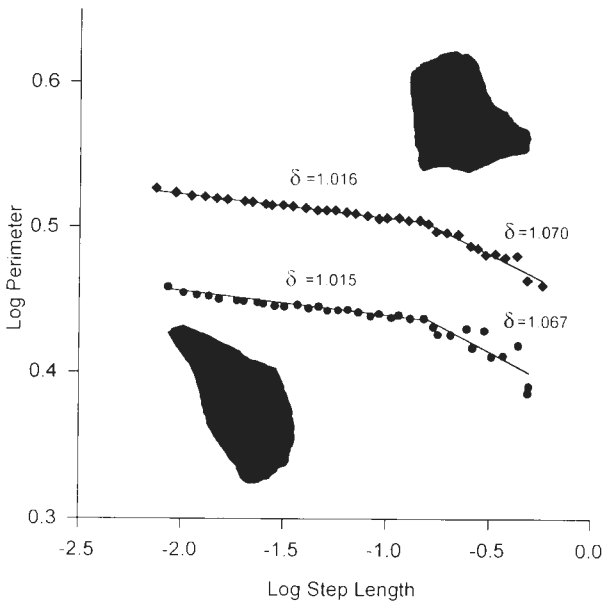

Figure 4. Richardson plots for two un-etched fine-particle cerussite profiles. Symbols described in text.

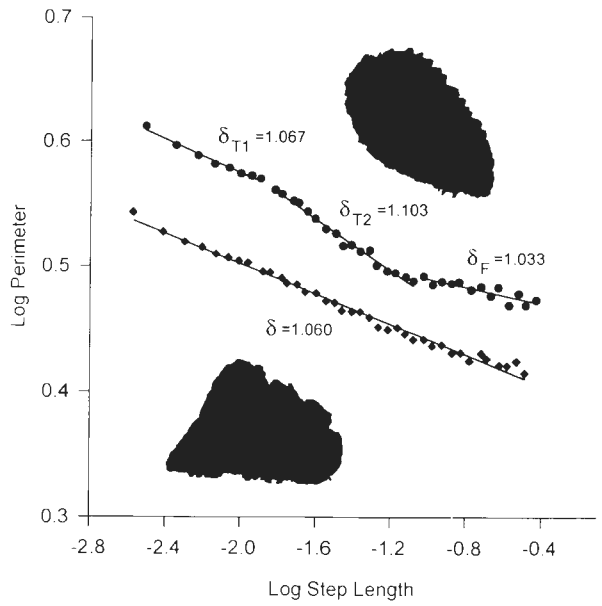

Figure 5. Richardson plots for two etched fine-particle cerussite profiles. Symbols described in text.

cerussite fracture grains with concave sections in the profile, a foreshortening of the perimeter at large step sizes will occur when the algorithm "cuts across" the concavity. Recurring embayments in the profile, which are accompanied by large scale projecting features, will be stepped around at smaller step sizes and will produce a characteristic structure fractal.

Richardson plots for the profiles of the etched particles revealed both single and multi-fractal forms. In the case of the multi-fractal plots, at the bigger step sizes the line segment either becomes steeper (an increase in δ) or less inclined (a decrease in δ) than the preceding line segment. Where δ increases, the texture component in the profile is stepped over and the structure elements which are present are stepped around giving a convex form to the Richardson plot. This segment describes the structure component and the associated fractal dimension is δ_S. The less steep (large step size) line segment is produced by particle profiles that exhibit a generalized ellipsoidal form (Figs. 3b and 3d). In the case of this type of profile, at the large step sizes, the texture elements are stepped over and the absence of major structure elements results in the macro-form of the outline being stepped around. This results in a less rapid progressive decrease in estimated perimeter, which produces an overall concave form in the Richardson plot. As this line segment does not report on prominent structural units in the outline, but follows the overall form of the profile, we refer to the associated fractal dimension as δ_F to distinguish it from δ_S which reports on major structural elements. The small scale irregularities (texture) in the profiles of two of the three multi-fractal grains are accounted for by a single line segment (δ_T), while the third (Fig. 3b) develops two textural fractal segments producing a tri-fractal plot (Fig. 5). The presence of two texture components arises from a distinctive spinescent element in the profile. In the resulting Richardson plot, the first line segment follows the fine texture of the grain outline (here designated as δ_{T1}) which varies little until the spinose component becomes important, giving rise to a second line segment (δ_{T2}). The acid etched particles which form single line segment Richardson plots display apparent textural and structural irregularities in their profiles. As there is no distinctive transition in these Richardson plots from a texture fractal to a structure fractal, and as the single fractal dimension reports on both small and large scale changes in profile roughness (consistently self similar), the single line segment simply describes the fractal dimension (δ) of the profile.

The post-acid treatment profiles differ significantly in terms of their fractal dimension compared to the pre-treatment grain outlines (Table 2). The more irregularly textured etched grains have consistently greater δ_T values ($\bar{x} = 1.083 \pm 0.02$) than the main line segment δ values obtained for the un-etched particles ($\bar{x} = 1.019 \pm 0.007$). The fractal dimension (δ) values for those etched profiles consisting of a single line segment Richardson plot ($\bar{x} = 1.095 \pm 0.035$) are also greater than δ values for the un-etched profiles. The δ values for the main line segment produced by the pristine profiles are significantly less than the δ, δ_T and δ_S values for the etched profiles at the $p = 0.01$ rejection level for the Mann-Whitney U statistic.

In situ single etching of fractured pyromorphite grains

Individual fractured pyromorphite fine-particles were imaged before and following an *in situ* immersion for 2 hours in 0.1 N hydrochloric acid. In pristine condition, the grains displayed a fracture surface morphology (Figs. 6a and 6b). After a continuous period of 2 hours under etching conditions, the grains were found to be extensively degraded. The pattern of corrosion was observed to be similar in both cases with each particle acquiring a platy appearance following the acid treatment (Figs. 6c and 6d). The rate of dissolution under these weak acid conditions was sufficient to permit factors such as fracture surfaces (and stresses caused by fracturing) and crystallographic form of the mineral to largely control the pattern of etching.

Pristine particle profiles and the rugged outlines created by the apparently overlapping plates which constitute the etched grains were used to assess the effects of the acid on grain shape. The Richardson plots obtained for the fine-particle pyromorphite prior to immersion in the weak acid depicted a single line segment, which essentially reports on an unvarying change in profile, roughness giving δ values of 1.025 and 1.021 (Table 3), closely correspond to the δ values obtained for the freshly fractured cerussite grains (Table 1). The conchoidal fracture of the pyromorphite particles is more regular than the sub-conchoidal or uneven fracture of the pristine cerussite grains, and this is the likely origin of the more irregular cerussite profiles which produce a second line segment at large step sizes in the Richardson plot. The post-dissolution values obtained for δ_T and δ_S (Table 3) were both higher than those for the un-etched profiles. The multifractal behavior observed in the Richardson plots obtained for the post-etch outlines clearly indicates that the etching process had resulted in a degree of ruggedness in the profile at the texture level, and had also revealed structural elements in the profile (Fig. 7).

In situ multiple etchings of a single fractured pyromorphite grain

An *in situ* multiple etching experiment was conducted to assess time-dependent changes in the value of δ for

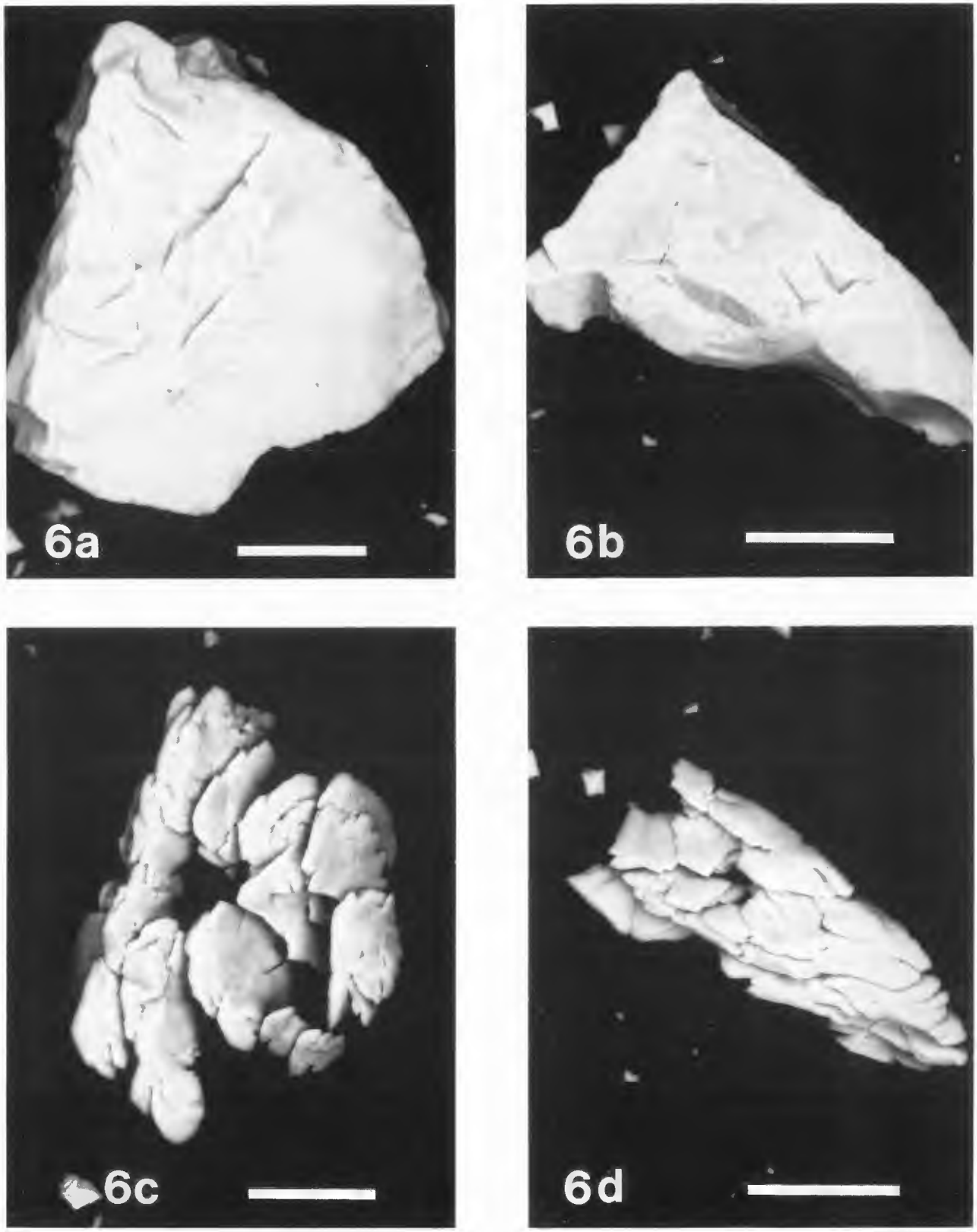

Figure 6. Backscattered electron images of two different fractured pyromorphite ($Pb_5(PO_4)_3Cl$) particles before (**a** and **b**) and following immersion (**c** and **d**) for 2 hours in 0.1 N HCl. Bars = 10 μm.

Table 4. Fractal dimension values for a single pyromorphite fine-particle repeatedly etched in 0.1 N HCl for periods of 15 minutes.

Time (minutes)	δ	δ_T (r^2)		δ_S (r^2)
		δ_{T1} (r^2)	δ_{T2} (r^2)	
0.00	1.029 (0.94)	-		-
45	1.054 (0.96)	-		-
180	-	1.058 (0.99)		1.086 (0.97)
210	-	1.065 (0.99)	1.172 (0.95)	1.256 (0.97)
240	-	1.055 (0.98)		1.194 (0.97)
270	-	1.049 (0.99)		1.165 (0.97)
300	-	1.049 (0.97)	1.137 (0.97)	1.286 (0.95)

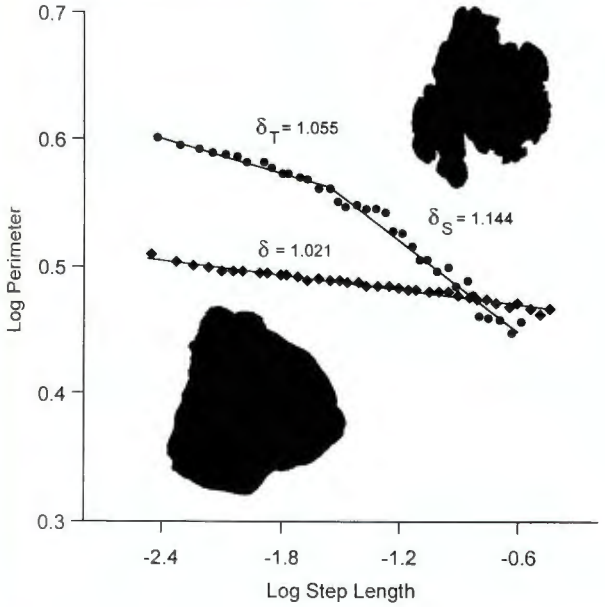

Figure 7. Richardson plots for a single pyromorphite fine-particle profile un-etched (bottom), and etched after immersion for 2 hours in 0.1 N HCl (top). Symbols described in text.

---

a lead fine-particle profile under acid dissolution conditions. Changes in the projected outline of a single fractured pyromorphite grain were recorded after repeated 15 minute periods of immersion in 0.1 N hydrochloric acid. Backscattered electron images of the grain at four selected time intervals (0, 45, 180 and 240 minutes) are presented in Figure 8. The dissolution process was observed to be discontinuous with active etching apparently occurring at certain times during the acid bathing and not at others. This may be a "wetability" phenomenon with incomplete exposure of the grain surface to the reagent at various intervals possibly effected by the multiple cycles of wetting and drying. For much of the initial phase of dissolution, the etching process appeared to be determined by the fracture pattern and crystal structure of the grain. Subsequently, specific portions of the particle were preferentially removed, leaving other parts of the grain relatively intact. Following an initial stage during which the particle became deeply ridged (Fig. 8b), parts of the grain became detached from the main body of the grain as the acid etched through thinner sections. The isolation of smaller parts of the particle resulted in the creation of a highly irregular outline for the main body of the grain (Fig. 9).

The values for the fractal dimension of the particle boundary were computed for the projected profile at 0, 45, 180, 210, 240, 270 and 300 minutes, and only for the outline of the main body of the grain. As with the fractured fine-particles described previously, the Richardson plot for the pristine grain reflected a simple Euclidean form with a prominent single line plot yielding a δ value of 1.029, which is comparable with values obtained for other un-etched fractured grains. Initial increases in profile roughness were matched by a concomitant increase in fractal dimension (Table 4). Subsequently, at t = 180 minutes, the most suitable fit for the Richardson plot data took the form of two line segments, by convention defined as δ_T and δ_S, and this continued to be the case with the exception of the profiles at 210 minutes and 300 minutes, when three line segments appeared the most appropriate fit for the data (Fig. 10). The profile is at its most convoluted at these times, and the two line segments at the smaller step sizes in the Richardson plots both follow the finer details in the grain outline. Hence, the fractal dimensions for these elements of the profile have been designated δ_{T1}

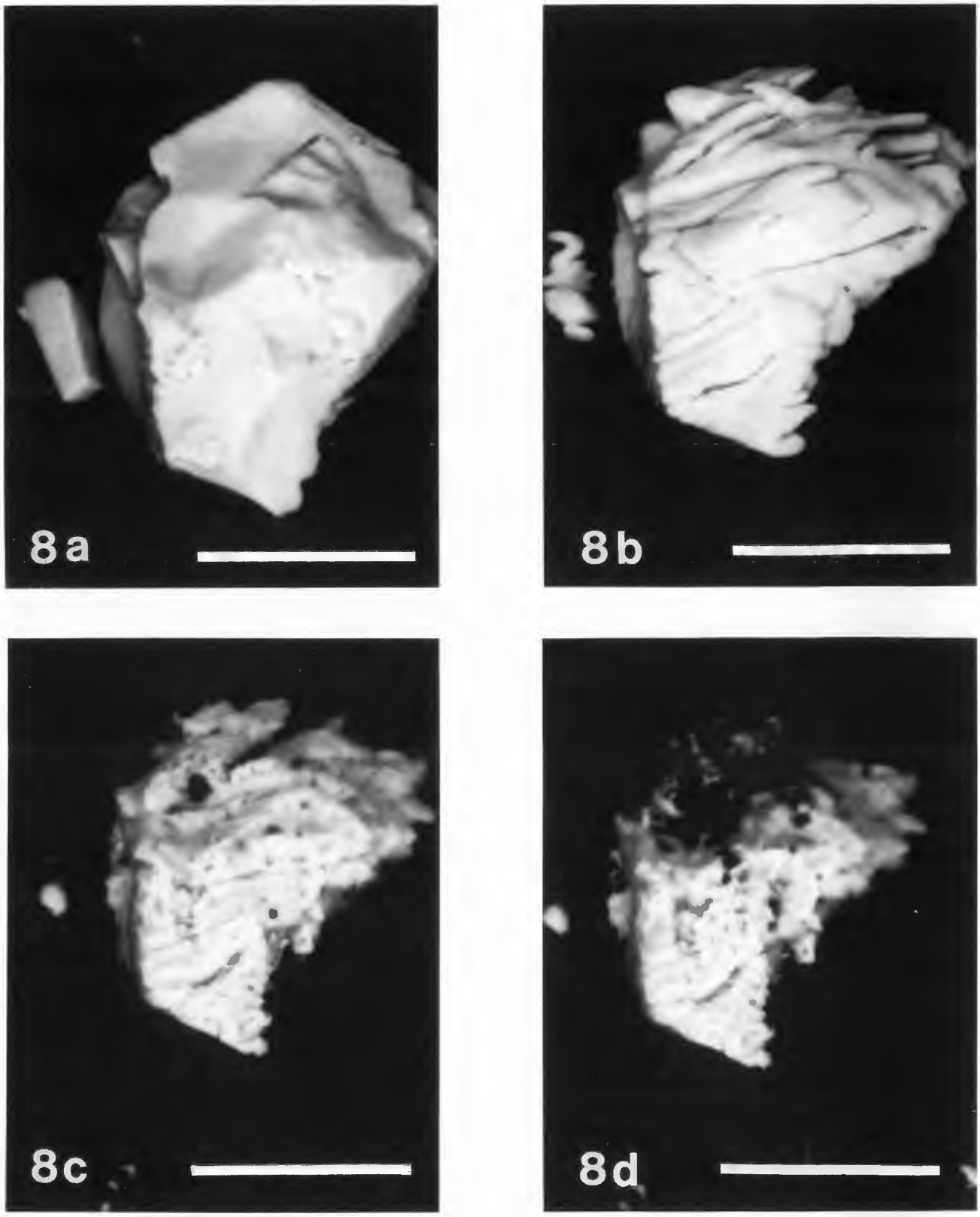

Figure 8. Backscattered electron images of a single pyromorphite fine-particle subjected to multiple sequential immersions in 0.1 N HCl at: 0 (**a**), 45 (**b**), 180 (**c**), and 240 minutes (**d**). Images tilted 45°. Bars = 10 μm.

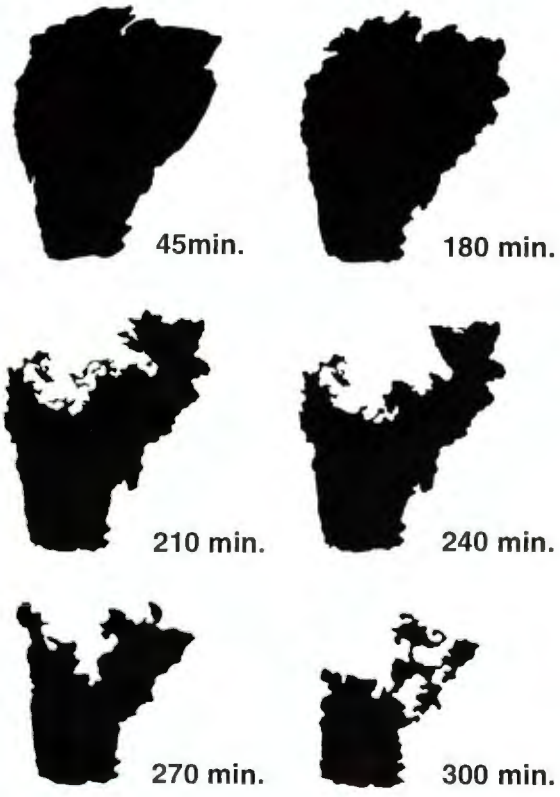

Figure 9. Outlines of a weak acid etched single pyromorphite fine-particle at time intervals: 45, 180, 210, 240, 270 and 300 minutes.

---

and δ_{T2}; for the third line segment, which reports on the larger (structural) components of the outlines, the fractal dimensions have been designated δ_S. The point of transition from textural to structural behavior in the Richardson plots varied between profiles. The break point separating δ_T from δ_S in the bi-fractal plots occurred in the step size range 0.025 - 0.040. The δ_{T2} segment in the tri-fractal plots emerged at smaller step sizes, and the δ_{T2} to δ_S transition occurred at larger step sizes.

Changes in the convex form of the sequence of Richardson plots ($\delta_T < \delta_S$) follow the changes in ruggedness of the pyromorphite particle outline. The sequence of profiles prior to and including that at t = 210 minutes demonstrate a progressive increase in rugosity and structural detail (Fig. 8) which gives rise to an incremental increase in δ_T and the emergence of multi-fractal behavior with progressive increases in δ_S. After t = 210 minutes, there is a simplification of the profile as the acid dissolution process removes textural and structural elements in the outline, leading to lower values of δ_T and δ_S. At t = 300 minutes, the etching process has again resumed dissolving portions of the

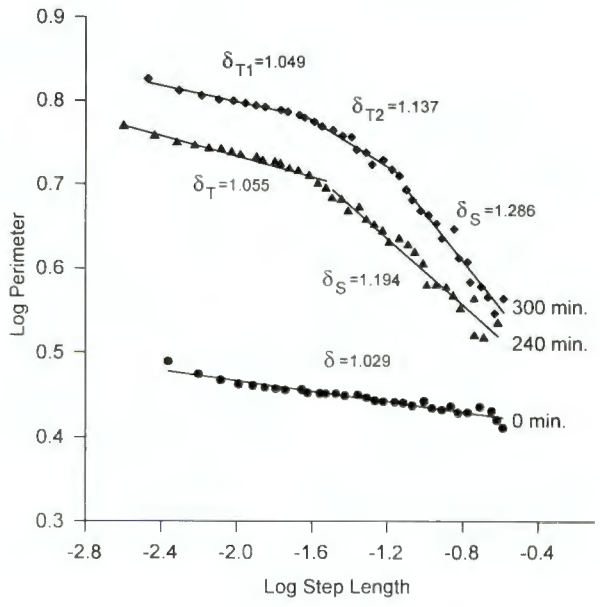

Figure 10. Richardson plots for an etched pyromorphite fine-particle profile at times: 0 minutes (●), 240 minutes (▲), and 300 minutes (◆).

---

main body of the grain, once more producing a convoluted profile that is multi-fractal in form. Thus, the dissolution sequence apparently involves an initial roughening of the profile, followed by the removal of structure and texture elements as the acid divides away parts of the particle from the main body of the grain which simplifies the outline; then, as the acid continues to etch the particle, the shape once more becomes irregular.

Discussion

Slopes obtained from the log-log plots of perimeter against side length for polygons approximating the outlines of acid etched lead fine-particles are consistently greater than the slopes obtained for un-etched fracture grains. This suggests that the computed values for the fractal dimension of particle profiles provides a potential method for differentiating between pristine and etched grains. The form of the Richardson plots generally fits the typology defined by Orford and Whalley (1987). Plots for pristine fracture grains, which generally consist of a single line segment of minimal slope, correspond to the first of three types of fractal behavior identified by this scheme. Multi-fractal plots which are concave in form were produced by individual etched cerussite grains, and plots of convex form generally by the degraded pyromorphite particle outlines. These forms of the Richardson plot conform to Types III and II fractal

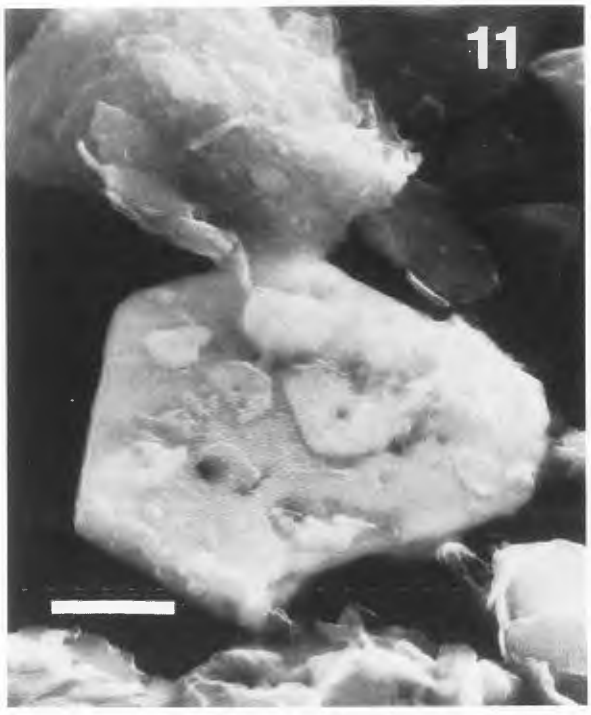

Figure 11. Secondary electron image of a lead particle from the surface layer of a soil from urban Syracuse, NY. The hexagonal form and lead composition suggests a lead carbonate grain probably derived from lead-based paint. Bar = 1 μm.

---

behavior respectively as defined by the scheme. In addition to these three types of fractal plot, etched cerussite profiles also produced single fractal dimension plots, and extensions of the convex and concave patterns in the form of tri-fractal plots were produced by both lead minerals. The relatively rapid dissolution of the cerussite fine particles tended to produce single line segments or bi-fractal concave Richardson plots. The lack of development of a consistently distinctive structural element can likely be attributed to the relatively unimpeded dissolution process at this pH. The less soluble pyromorphite grains, following a 2 hour immersion in the dilute acid, evolved profiles with obvious structural components which relate to factors that include: fracture patterns, crystal structure and mineral solubility, which produced Type II Richardson plots. The pyromorphite particle, which was subjected to a repeated cycle of immersion, drying, and SEM examination, displayed a modified pattern of etching that appears to also be related to the crystalline nature of the grain with pitting of the grain surface (Fig. 8). In the first instance, the etching process created an increasingly intricate profile, then as textural and structural protuberances were dissolved or parted away from the original grain (forming separate fine particles) the level of detail diminished. This simplifying of the profile survived temporarily to be replaced by a more convoluted outline following additional etching. The irregular dissolution of the grain that produced both texture and structure features generates, as might be expected, a sequence of Type II Richardson plots. A somewhat similar sequence of events to this has been reported by Kaye (1989) in a light microscopic study of the hydrochloric acid dissolution of an aluminum fine-particle. The changing δ values for the profile of the aluminum particle were considered to reflect a change from a rough outline (the initial state of the grain) to a relatively even, acid smoothed profile, which was then superseded by a more rugged profile as the acid further attacked the grain.

In situ and *ex situ* chemical dissolution experiments with fine-particulate lead have demonstrated that the profiles of pristine and etched grains have characteristically different fractal dimensions. This implies that it may be possible to use fractal dimension as a grain shape descriptor to differentiate between these two types of particle profile under various dissolution conditions. If lead particle profiles can be characterized in terms of fractal dimension, this may prove to be a useful indicator of the degree of roughening (and hence dissolution) of various lead particle types in *in vitro* biosolubility experiments designed to simulate conditions in the human gastrointestinal tract. Also, fractal dimension values obtained for lead particles in environmental media (dusts, soils, aerosols) may prove to be a useful descriptor of chemical history. For example, the outline of the pitted soil lead particle in Figure 1 has a δ value of 1.108 (r^2 = 0.95). In comparison, the soil lead particle in Figure 11, which is also from an urban surface soil and which has an un-etched outline, has a δ value of 1.019 (r^2 = 0.92). Both soil lead particles when analyzed by X-ray microanalysis using a beryllium window detector were composed only of lead (indicating a lead metal, oxide or carbonate composition) and are effectively chemically indistinguishable under these analytical conditions. The composition and the hexagonal morphology would indicate that the un-etched grain is probably a lead carbonate particle derived from old lead-based paint. While it may be possible to distinguish between compositionally similar soil lead particles on the ruggedness of their profiles, the possibility of using fractal dimension as a discriminator of chemical environment or residence time in such an environment has yet to be investigated.

Acknowledgements

We are indebted to Drs. J.L. Abraham and W. Patterson for their advice and M. Barcza for a careful

reading of the manuscript. We would also like to thank the reviewers for bringing many important points to our attention.

References

Cotter-Howells J, Thornton I (1991) Sources and pathways of environmental lead to children in a Derbyshire mining village. Environ Geochem Health **13**: 127-135.

Davis A, Ruby MV, Bergstrom PD (1992) Bioavailability of arsenic and lead in soils from the Butte, Montana, mining district. Environ Sci Technol **26**: 461-468.

Davis A, Drexler JW, Ruby MV, Nicholson A (1993) Micromineralogy of mine wastes in relation to lead bioavailability, Butte, Montana. Environ Sci Technol **27**: 1415-1425.

Day JP, Fergusson JE, Chee TM (1979) Solubility and potential toxicity of lead in urban street dust. Bull Environ Contam Toxicol **23**: 497-502.

Duggan MJ, Inskip MJ (1985) Childhood exposure to lead in surface dust and soil: A community health problem. Public Health Rev **13**: 1-54.

Gulson BL, Davis JJ, Mizon KJ, Korsch MJ, Law AJ, Howarth D (1994) Lead bioavailability in the environment of children: Blood lead levels in children can be elevated in a mining community. Arch Environ Health **49**: 326-331.

Hayward J, Orford JD, Whalley WB (1988) Three implementations of fractal analysis of particle outlines. Comput Geosci **15**: 199-207.

Johnson DL, Hunt A (1995) Analysis of lead in urban soil by computer assisted SEM/EDX-method. Development and early results. In: Lead in Paint, Soil and Dust: Health Risks, Exposure Studies, Control Measures, Measurement Methods, and Quality Assurance, ASTM STP 1226. Beard ME, Iske SDA (eds.). American Society for Testing and Materials, Philadelphia, PA. pp. 283-299.

Katrinak KA, Rez P, Perkes PR, Buseck PR (1993) Fractal geometry of carbonaceous aggregates from an urban aerosol. Environ Sci Technol **27**: 539-547.

Kaye BH (1989) A Random Walk Through Fractal Dimensions. VCH Publishers, Weinheim, Germany. pp. 57-174.

Kaye BH (1993) Exploring the Patterns of Chaos and Complexity. VCH Publishers. pp. 334-340.

Kaye BH, Clark GG, Leblanc JE, Trottier RA (1987) Image analysis procedures for characterizing the fractal dimension of fine particles. Part Charact **4**: 3-66.

Kaye BH, Clark GG, Kydar Y (1993) Strategies for evaluating boundary fractal dimensions by computer aided image analysis. Part Part Syst Charact **11**: 411-417.

Kindratenko VV, Van Espen PJM, Treiger BA, Van Grieken RE (1994) Fractal dimensional classification of aerosol particles by computer controlled scanning electron microscopy. Environ Sci Technol **28**: 2197-2202.

Mandelbrot BB (1967) How long is the coast of Britain? Statistical self-similarity and fractional dimension. Science **156**: 636-638.

Mandelbrot BB (1982) Fractal Geometry of Nature. W.H. Freeman, San Francisco, CA. pp. 25-83.

Medalia AI (1970-71) Shape factors of particles. Powder Technol **4**: 117-138.

Orford JD, Whalley WB (1983) The use of fractal dimension to quantify the morphology of irregular-shaped particles. Sedimentology **30**: 655-668.

Orford, JD, Whalley WB (1987) The quantitative description of highly irregular sedimentary particles: The use of the fractal dimension. In: Clastic Particles: Scanning Electron Microscopy and Shape Analysis of Sedimentary and Volcanic Clasts. Marshall JR (ed.). Van Nostrand, New York. pp. 267-280.

Rabinowitz MB (1993) Modifying soil lead bioavailability by phosphate addition. Bull Environ Contam Toxicol **51**: 438-444.

Rickard DT, Nriagu JO (1978) Aqueous environmental chemistry of lead. In: The Biogeochemistry of Lead in the Environment. Nriagu JO (ed.). Elsevier/ North Holland Biomedical Press, Amsterdam, The Netherlands. pp. 219-284.

Ruby MV, Davis A, Kempton JH, Drexler JW, Bergstrom PD (1992) Lead bioavailability: Dissolution kinetics under simulated gastric conditions. Environ Sci Technol **26**: 1242-1248.

Schwartz H, Exner E (1980) The implementation of the concept of fractal dimensions on a semi-automatic image analyzer. Powder Technol **27**: 207-213.

Xie Y, Hopke PK, Casuccio G, Henderson B (1994) Use of fractal dimension to quantify airborne particle shape. Aerosol Sci Technol **20**: 161-168.

Discussion with Reviewers

X. Maldague: Why was particle dissolution conducted both *ex situ* and *in situ*? Please elaborate on this point.
Authors: The two methods take different approaches to particle dissolution. The *in situ* procedure has the advantage of allowing the same particle(s) to be re-examined after one or more exposures to a test reagent. The *ex situ* approach, which provides data on populations of similar particles, is less labor intensive since time consuming particle re-location is avoided. Within the experimental framework discussed here, both methods make it is possible to follow changes in grain shape that result from exposure to a chemical environment conducive to particle dissolution.

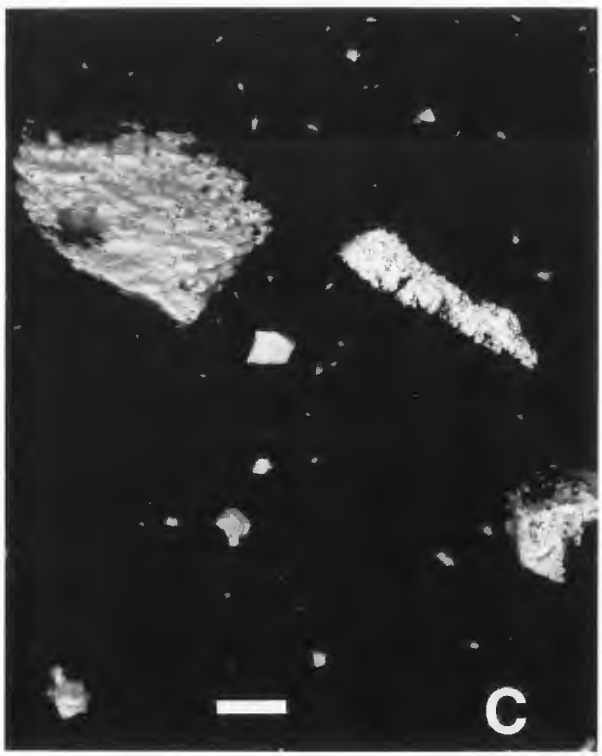

Figure A. Backscattered electron images of several different fractured pyromorphite particles following a 2 hour immersion in 0.1 N HCl. Bar = 10 μm.

Figure B. Backscattered electron image of several fractured pyromorphite fine-particles prior to immersion in 0.1 N HCl. Bar = 10 μm.

Figure C. Backscattered electron image of the same set of pyromorphite fine-particles (Fig. B) following repeated 15 minute immersions in 0.1 N HCl for a total of 240 minutes. Bar = 10 μm.

X. Maldague: The phrase "multiple grey scale to black and white binary images" is unclear, especially if digital format is involved since this implies binary imaging directly, unless images were previously saved under various formats such as TIF, etc. Is that what is meant?
Authors: Prior to image capture the backscattered electron signal strength was optimized in terms of contrast and brightness to maximize the separation between the substrate and the high atomic number lead features and preserve a range of gray levels sufficient to illustrate the surface topography of the grains. Images recorded photographically were subsequently scanned at a resolution

of 400 dpi, without any change in contrast and brightness, and stored as TIFF files. Grey scale digital images acquired directly from the SEM were collected at a resolution of 1024 x 800 pixels and 124 grey levels and were also saved in TIFF format. Conversion to a binary image was accomplished using commercially available image processing software by thresholding the image at the point on the grey scale histogram where the transition occurred from black background to the much higher intensity particle region of the image. Finally, before determining the x,y addresses of the boundary pixels, the image was re-sized (generally by cropping excess off the feature background) to fit within a 700 x 700 pixel array.

W.B. Whalley: How many grains have been used in the experiments, only those seen? Mineralogical variability, e.g., cleavages, might give different etching results according to where the digitized surface was related to zones of maximized or minimized etching.
Authors: The results described here are preliminary and are presented as proof of concept. Our discussion is restricted to data from 23 profiles from 15 particles (sequential acid etching producing several outlines). The question of sample versus analytical variability is not easily addressed with this initial data set. Etching of the grains will be related to crystal structure, fracturing, defects and various other factors. However, the data presented are not for unrepresentative particles; we did observe the same dissolution effects as those reported in other grains which were either not imaged at time zero in the single *in situ* etching study or not imaged in detail throughout the sequential *in situ* etching study. By way of illustration, the pyromorphite particles in Figure A, which were imaged at the conclusion of the 2 hour *in situ* weak HCl etching, have the same post acidification form as those set out in Figure 6. Similarly, the larger un-etched pyromorphite particles in Figure B (including the grain followed in detail in Figure 8), which were repeatedly immersed *in situ* in dilute HCl, displayed characteristically similar rugged outlines at subsequent time intervals (Fig. C). To assess how the variability in the projected profiles of these grains effects the fractal dimension calculations will require data from a larger number of grain outlines.

R. Thibert: Could you suggest a better approach than visual inspection in the evaluation of the break point to distinguish the presence of multifractal behavior?
Authors: For line segment analysis related to other applications, we have experimented with a "pipe" algorithm. When the Richardson plot points are visualized as joined into a rigid line, a rectangle (pipe) of user specified length and width is moved sequentially down the line from one end until no more of it can "fit" within the selected dimensions. If the length requirement has been satisfied, a segment is then removed and the process repeated on the remaining points with removal of additional segments as needed. This approach can identify the number of segments in a Richardson plot, but accurate location of segment break points requires an iterative procedure with movement of the "pipe" in both directions on the various segments. Discontinuities in the Richardson plot, such as those exhibited by the Medalia reference feature, present additional problems with its implementation; but we remain convinced that if visual inspection can deselect such curve regions, programming code with appropriate rule-based structures can also be constructed.